JOURNAL OF SYNCHROTRON RADIATION

ISSN 1600-5775

Synchrotron study of metal localization in *Typha latifolia* L. root sections

Yu Qian,[a]‡ Huan Feng,[a]* Frank J. Gallagher,[b] Qingzhi Zhu,[c] Meiyin Wu,[d] Chang-Jun Liu,[e] Keith W. Jones[f] and Ryan V. Tappero[f]

[a]Department of Earth and Environmental Studies, Montclair State University, Montclair, NJ 07043, USA, [b]Environmental Planning and Design Program, Department of Landscape Architecture, Rutgers, The State University of New Jersey, New Brunswick, NJ 08901, USA, [c]School of Marine and Atmospheric Science, State University of New York, Stony Brook, NY 11794, USA, [d]Department of Biology and Molecular Biology, Montclair State University, Montclair, NJ 07043, USA, [e]Biosciences Department, Brookhaven National Laboratory, Upton, NY 11973, USA, and [f]Photon Sciences Directorate, Brookhaven National Laboratory, Upton, NY 11973, USA.
*Correspondence e-mail: fengh@mail.montclair.edu

Received 13 March 2015
Accepted 15 September 2015

Edited by S. M. Heald, Argonne National Laboratory, USA

‡ Current Address: School of Ecology and Environmental Sciences, Yunnan University, Kunming, Yunnan 650091, People's Republic of China.

Keywords: synchrotron μXRF; root metal uptake and transportation; iron plaque; *Typha latifolia* L.; wetland.

Supporting information: this article has supporting information at journals.iucr.org/s

Understanding mechanisms that control plant root metal assimilation in soil is critical to the sustainable management of metal-contaminated land. With the assistance of the synchrotron X-ray fluorescence technique, this study investigated possible mechanisms that control the localization of Fe, Cu, Mn, Pb and Zn in the root tissues of *Typha latifolia* L. collected from a contaminated wetland. Metal localizations especially in the case of Fe and Pb in the dermal tissue and the vascular bundles were different. Cluster analysis was performed to divide the dermal tissue into iron-plaque-enriched dermal tissue and regular dermal tissue based on the spatial distribution of Pb and Fe. Factor analysis showed that Cu and Zn were closely correlated to each other in the dermal tissues. The association of Cu, Zn and Mn with Fe was strong in both regular dermal tissue and iron-plaque-enriched dermal tissue, while significant ($p < 0.05$) correlation of Fe with Pb was only observed in tissues enriched with iron plaque. In the vascular bundles, Zn, Mn and Cu showed strong association, suggesting that the localization of these three elements was controlled by a similar mechanism. Iron plaque in the peripheral dermal tissues acted as a barrier for Pb and a buffer for Zn, Cu and Mn. The Casparian strip regulated the transportation of metals from dermal tissues to the vascular bundles. The results suggested that the mechanisms controlling metal localization in root tissues varied with both tissue types and metals.

1. Introduction

Urban soil contamination has increased dramatically in recent decades due to anthropogenic activities (Qian *et al.*, 2011; Wuana & Okieimen, 2011; Desouki & Feng, 2012; Luo *et al.*, 2012). Lead (Pb), copper (Cu), manganese (Mn) and zinc (Zn) are contaminants commonly find in urban soil. Once they enter the soil, these metals cannot be degraded and tend to accumulate in the soil and pose potential risks to urban ecological stability and human health. Urban brownfields are a concern specifically because they are in densely populated areas and difficult to revitalize (French *et al.*, 2006; Gallagher *et al.*, 2008; Luo *et al.*, 2012). Plants are transplanted in abandoned brownfields to mitigate soil metal contamination, improve urban ecosystem stability and remediate soil metal contamination (McKenna, 1998; French *et al.*, 2006; Dickinson *et al.*, 2009; Desouki & Feng, 2012;). *Typha latifolia* L. (broadleaf cattail) is a wetland plant that is widely used for

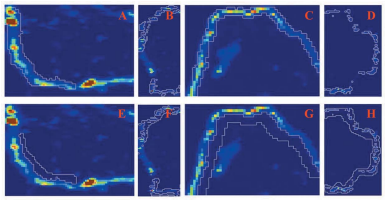

wetland restoration, eutrophic lake clean-up and wastewater effluent treatment (Ye *et al.*, 1997, 1998; Sasmaz *et al.*, 2008; Calheiros *et al.*, 2009). Previous field studies identified *T. latifolia* L. as a plant species that is capable of tolerating soil with extremely high metal concentration (McNaughton *et al.*, 1974), which makes it an ideal candidate for metal phytoextraction from the contaminated wetlands to meet remediation purpose (McNaughton *et al.*, 1974; Ye *et al.*, 1997, 2001; Sasmaz *et al.*, 2008; Brunham & Bendell, 2010; Grisey *et al.*, 2012; Klink *et al.*, 2012). A better understanding of metal uptake and translocation processes in the plant will benefit future application of *T. latifolia* L. in environmental management projects.

The uptake and translocation of metals by plant root is controlled by many mechanisms that vary with root tissues. On the surface of wetland plant root, a layer of amorphous Fe hydroxide named as iron plaque is commonly observed (Ye *et al.*, 1997). The negative surface charge of iron plaque makes it capable of adsorbing or co-precipitating metal(loid)s (Ye *et al.*, 1998, 2001). Located at the interface between soil pore water and root surface dermal tissues, iron plaque plays a role either as a buffer that enhances metal uptake efficiency or as a barrier that restricts the transportation of metals at the root surface (Tripathi *et al.*, 2014). On the peripheral part of the root are dermal tissues, which either uptake metal ions in soil pore water freely through passive diffusion in the apoplast system or uptake and transport metals selectively into the symplast system under the assistance of selective cell membrane transporters (Taiz & Zeiger, 2010; Marschner, 2012). When metals reach the vascular bundles in the middle of the root, the transportation of substances in the apoplast is blocked by the Casparian strip and prevents them from entering the vascular bundles. Only metals in the symplastic system can enter the vascular tissue and be further transported to the plant shoot (Brennan & Shelley, 1999; Clemens & Palmgren, 2002; Rascio & Navari-Izzo, 2011). Localization of metals in root tissues indicates the possible mechanisms a plant root takes to regulate metal uptake and transportation processes (Marschner, 2012).

Recently, advanced high-resolution analytical techniques have provided micro-scale metal localization information and supported plant metal uptake and translocation mechanisms studies. For example, Lyubenova *et al.* (2012, 2013) applied micro-proton-induced X-ray emission (micro-PIXE) to analyze the spatial distribution of 18 elements in *T. latifolia* L. tissues and observed tissue-specific distribution patterns of these elements. Synchrotron X-ray absorption near-edge microstructure spectroscopy (XANES) measurement for identification of Pb and Fe speciation on *T. latifolia* L. roots surface showed that Pb(II) and Fe(III) are the major species in the iron plaque in the root epidermis (Feng *et al.*, 2013). In this study, we aimed to investigate the mechanisms that control the localization of Cu, Fe, Pb, Mn and Zn in *T. latifolia* L. root tissues and understand uptake and translocation mechanisms in *T. latifolia* L. root for metal assimilation.

2. Methodology

2.1. Study site

The study area was chosen in an urban brownfield within Liberty State Park, New Jersey, USA, with an area of 1 km^2. This region was once used for railway transportation and coal storage for a century. As a result of previous industrial activities, high soil metal concentrations were found in this area (Gallagher *et al.*, 2008; Qian *et al.*, 2012). The specific site for this study was chosen at a wetland site which is part of a storm water drainage ditch. Previous studies showed that the total soil metal concentrations of Cu, Pb and Zn in this wetland were 124 $\pm$ 51 $\mu g\ g^{-1}$, 453 $\pm$ 266 $\mu g\ g^{-1}$ and 309 $\pm$ 125 $\mu g\ g^{-1}$, respectively, which were all above the background levels in New Jersey (Cu: 14 $\mu g\ g^{-1}$; Pb: 35 $\mu g\ g^{-1}$; Zn: 22 $\mu g\ g^{-1}$; EPA, 2005) and indicated the site was highly contaminated (Gallagher *et al.*, 2008).

2.2. Sample collection and process

Because plants in the growing season have the highest metabolism rate and root-to-shoot translocation rate, this period is selected to conduct root metal uptake/translocation mechanism study. The growing season of *T. latifolia* L. usually lasts from May to July each year (Tursun *et al.*, 2011). Plant samples were collected from the study site in the growing season in 2010 and 2011 along the edge of a storm water drainage ditch. After collection, the samples were immediately transported to Montclair State University for laboratory treatment. Bulk soils on the plant roots were removed by hand initially, then the soil particles were rinsed off gently with tap water and finally with distilled-deionized water. To prepare the samples for synchrotron X-ray fluorescence (XRF) analysis, fresh roots were excised from the plant and then embedded in the cryo-embedding compound and then frozen to a solid at an optimal cutting temperature of 253 K (Feng *et al.*, 2013). The root sections of 30 µm thickness were then cut from the frozen samples with a cryotome (Cryostat CM1950, Leica Microsystems) and mounted on a 25 mm $\times$ 76 mm quartz microscope slide (SPI Supplies®). Two root sections were prepared from one plant collected in each year. Four root sections were made in total. The prepared root sections were stored at 277 K before synchrotron XRF analysis (Zhang *et al.*, 2011).

2.3. Synchrotron analysis

Synchrotron micro X-ray fluorescence (µXRF) analysis on the four root sections was conducted at the X27A beamline workstation at the National Synchrotron Light Source at Brookhaven National Laboratory (Upton, NY, USA). The energy range was fixed at 13.5 keV to excite fluoresces of Cu, Fe, Pb, Mn and Zn simultaneously. Optical images of the root sections were collected with an optical microscope before synchrotron XRF analysis. Before the analysis started, the slide mounted with the samples was oriented at 45° to the beam and a 13-element Canberra Ge array was used to

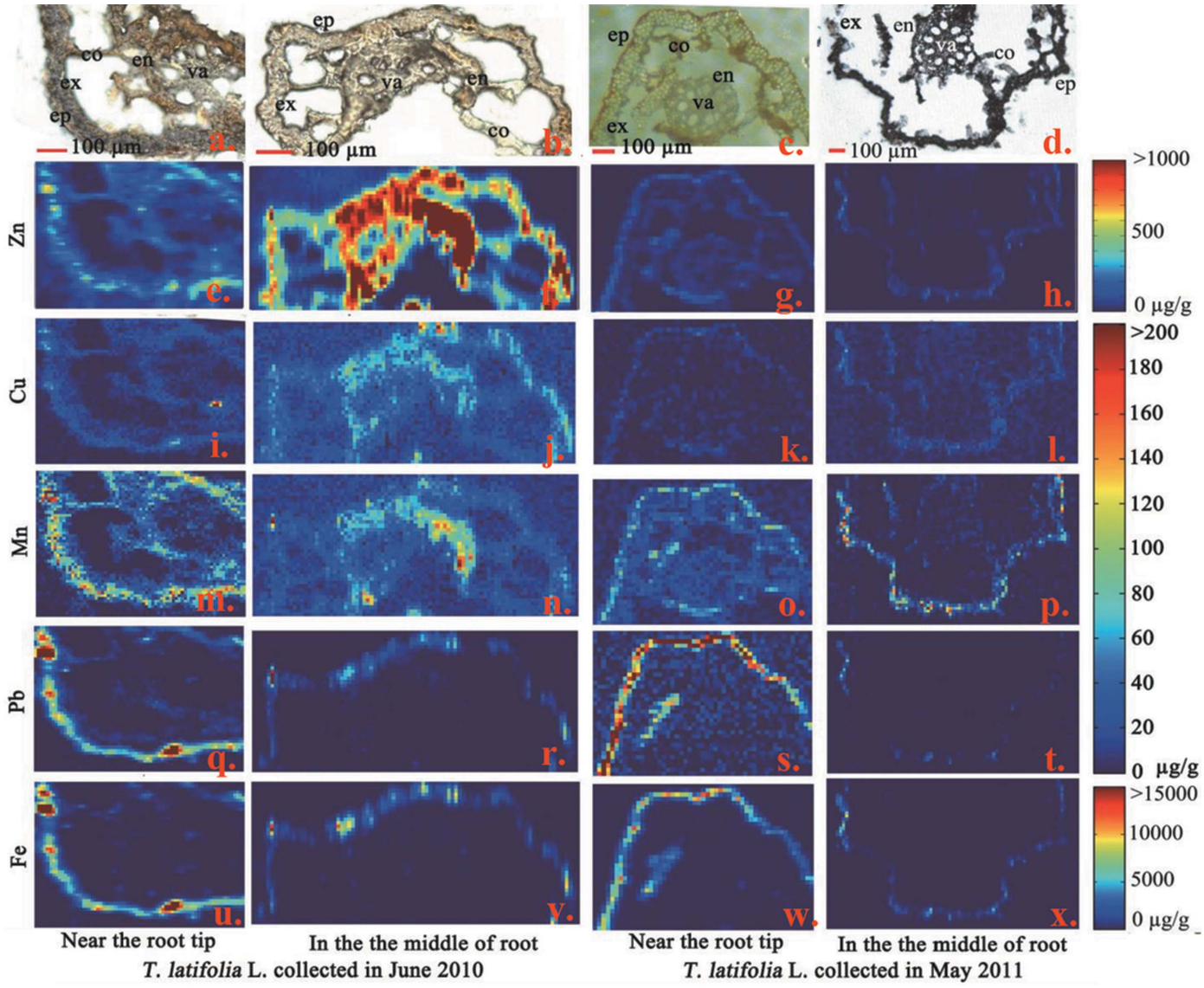

Figure 1
Optical images and concentration (μg g^{-1}) spatial distribution of Cu, Mn, Pb, Fe and Zn in *T. latifolia* L. root sections in the tip and the middle of roots collected in 2010 and 2011. ep: epidermis; ex: exodermis; co: cortex; en: endodermis; ca: Casparian strip; va: vascular tissues [(*a*)–(*d*) optical images of root tissue sections; (*e*)–(*h*) spatial distribution of Zn; (*i*)–(*l*) spatial distribution of Cu; (*m*)–(*p*) spatial distribution of Mn; (*q*)–(*t*) spatial distribution of Pb; (*u*)–(*x*) spatial distribution of Fe].

collect an elemental map with a step size of 10 μm and a dwell time of 7 s (Fig. 1). The synchrotron XRF data collection was carried out at the beamline workstation and then processed at Montclair State University. NIST Standard Reference Material (SRM) 1832 and 1833 were analyzed along with the samples during each synchrotron XRF measurement.

Longitudinal mapping of metal (Cu, Fe, Mn and Zn) distributions in the root specimens was carried out at the NSLS X26A beamline using a synchrotron μXRF microprobe. The X-ray energy was set at 13.5 keV. The beam size on the sample was 7 μm × 10 μm with a step size of 15 μm. The attenuation of the incident X-rays and outgoing X-rays was relatively low so that the entire thickness of the root was sampled with varying efficiencies.

2.4. Root anatomy

Five different types of root tissue could be identified based on optical images of the root section: epidermis, exodermis, cortex, endodermis and vascular bundles [Figs. 1(*a*)–1(*d*)].

2.5. Data processing and analysis

2.5.1. Tissue data extraction. The original micro-scale concentration data of metals (Cu, Zn, Mn, Pb and Zn) in each root section was saved as a matrix and presented as a two-dimensional map (Fig. 1). Each pixel in the synchrotron XRF map represents metal concentration in the root section voxel with a resolution of 10 μm × 10 μm for the 2010 samples or 20 μm × 20 μm for the 2011 samples. Based on root anatomy morphology observed in the optical images, the root dermal

tissues and the vascular bundles (surrounded by endodermis) were identified (see Fig. S1 of the supporting information) and the data were extracted from the original XRF map using MATLAB (The MathWorks Inc., version 7.1.0.246). The extracted matrix data were then transformed into linear form for further statistical analysis.

2.5.2. Identification of iron-plaque-enriched root dermal tissues. Many studies have proved that iron plaque exists in peripheral dermal tissues and it can effectively adsorb metals such as Pb, Mn, Zn and Cu (Greipsson & Crowder, 1992; St-Cyr & Campbell, 1996; Ye *et al.*, 1997). Iron plaque and regular dermal tissue accumulate metals through different mechanisms. Therefore, it is critical to separate the iron-plaque-enriched dermal tissues from regular dermal tissues in peripheral dermal tissues before analyzing the relationship between the metals.

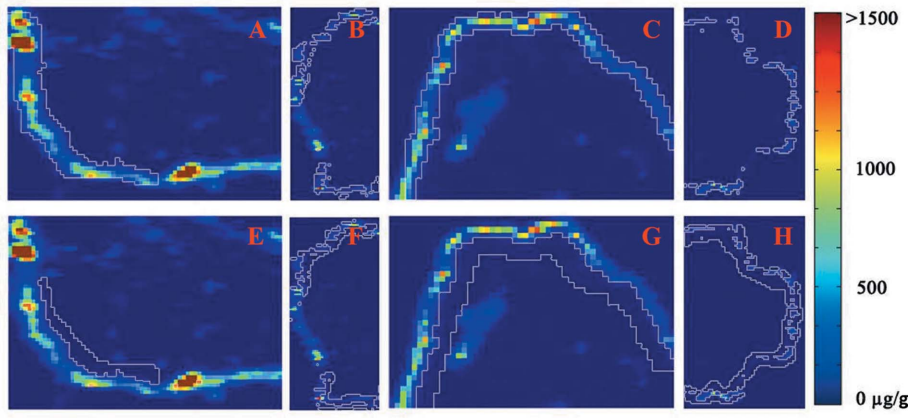

Figure 2
Iron plaque region and regular dermal tissue region identified by cluster analysis in the dermal tissues of four root sections [(*a*)–(*d*) CA1 iron plaque region; (*e*)–(*h*) CA2 regular dermal tissue]. The concentration scale bar indicates the concentration of Fe in the XRF map; the regions traced by the white line indicate identified clusters.

High sorption of Pb by iron plaque on *Iris pseudacorus* L. root surface has already been reported (Zhong *et al.*, 2010). Liu *et al.* (2011) also indicate that iron plaque can increase the sequestration of Pb on *Oryza sativa* L. root surface. The similar spatial distribution of high concentration of Pb [Figs. 1(*q*)–1(*t*)] and Fe [Figs. 1(*u*)–1(*x*)] in *T. latifolia* L. dermal tissues is consistent with the observation in the above studies that there is strong association between Pb and iron plaque. Therefore, spatial distributions of Pb and Fe in the dermal tissue were used as an indicator of the existence of iron plaque in the dermal tissue.

Hierarchical cluster analysis was performed based on the spatial distributions of Pb and Fe in dermal tissues of each sample to investigate the close association between metal distributions in the dermal tissues and identify dermal tissue regions enriched in iron plaque. The type of joining algorithm used to amalgamate clusters was Ward's method and the metric for measuring the distance between the metals in each case was the Euclidean distance (Burns & Burns, 2008; McDonald, 2009). Root dermal tissues are divided into two clusters: iron-plaque-enriched dermal tissues (in short, iron plaque) (CA1) and regular dermal tissues (CA2) (Fig. 2).

2.5.3. Data analysis. The metal concentration from synchrotron µXRF measurement was originally in units of counts per second (cps). It was then converted to units of µg g^{-1} by calibrating the samples against the NIST SRM 1832 and 1833 thin glass film on polycarbonate for XRF spectrometry, provided that the root tissue density was 1.0 µg g^{-1}. This calibration method did not account for differences in sample matrix and assumed that the absorption correction was not necessary, which works well for thin samples of uniform thickness (Feng *et al.*, 2013, 2015). In statistical analysis, factor analysis was applied to identify the inherent association between the spatial distribution of Cu, Mn, Fe, Pb and Zn in both dermal tissues and vascular bundles. Simple linear regression analysis was performed to explore the relationship between metals. MATLAB, SYSTAT (SYSTAT Software Inc.) and JMP (JMP®) were applied for statistical analyses of the data.

3. Result

3.1. Root anatomy analysis

Fig. 1 shows the anatomy structure of root sections of *T. latifolia* L. Five different types of root tissue could be identified, which are epidermis, exodermis, cortex, endodermis and vascular bundles. Epidermis, exodermis and the tissue between are considered as dermal tissues [Fig. 1(*a*)–1(*d*), ep, ex]. Dermal tissue maintains the selectivity of root uptake from soil by taking up water and nutrients and avoiding unwanted compounds like toxic substances and soil-borne pathogens (Schreiber & Franke, 2011). Cortex tissues include several layers of cells with thin cell walls [Fig. 1(*a*)–1(*d*), co]. In the middle of the root is a vascular bundle, surrounded by a layer of endodermis with the suberized Casparian strip [Fig. 1(*a*)–1(*d*), en and va]. The vascular bundles selectively transport substances from root cortex tissues and upload the substances to stems and shoots of the plant (Schreiber & Franke, 2011).

3.2. Metal localizations in dermal tissues and vascular bundles

As indicated by the coefficient of variance for each element in Table 1, metal localization in root dermal tissues and vascular bundles are highly heterogeneous. Also, the concentration of one metal element in the same type of tissue from each sample is different (Fig. 1 and Table 1), suggesting that the accumulation of metals in root is inconsistent. Nevertheless, the spatial distribution pattern of metals is still very similar between the four samples (Fig. 1, ep, ex).

In the dermal tissues, the concentration of Fe is the highest among all of the five elements ranges from 374 ± 836 µg g^{-1} to 3709 ± 4806 µg g^{-1} (Table 1, Fig. 1). The coefficient of

Table 1
Metal concentrations [mean ± standard deviation (SD)] (μg g^{-1}) and ranges (minimum, median, maximum) (μg g^{-1}) of Cu, Fe, Mn, Pb and Zn in the root sections collected in the tip and middle of *T. latifolia* L. in 2010 and 2011.

BDL = below detection limit.

		Dermal tissues						Vascular bundles					
Sample	Element	*n*	Min (μg g^{-1})	Max (μg g^{-1})	Median (μg g^{-1})	Mean (μg g^{-1})	c.v.	*n*	Min (μg g^{-1})	Max (μg g^{-1})	Median (μg g^{-1})	Mean (μg g^{-1})	c.v.
2010 (I)	Fe†		BDL	33464	2373	3709	1.30		BDL	1661	30.7	88.0	1.87
	Cu		BDL	76.0	16.9	18.7	0.59		BDL	41.8	9.46	11.1	0.74
	Zn†	531	19.7	666	179	188	0.54	836	BDL	453	73.7	104	0.78
	Mn†		BDL	240	50.5	56.9	0.70		BDL	138	15.9	25.7	1.07
	Pb†		BDL	916	38.2	62.2	1.65		BDL	30.6	BDL	2.22	2.05
2010 (II)	Fe†		n.d.	14667	328	862	1.82		BDL	772	59.0	75.9	1.08
	Cu†		3.68	212	41.5	44.2	0.47		BDL	96.2	40.3	41.8	0.37
	Zn†	659	29.6	1466	468	510	0.51	541	BDL	4027	742	964	0.69
	Mn†		1.33	203	28.0	29.6	0.55		BDL	199	38.9	50.8	0.67
	Pb†		BDL	422	3.01	9.63	2.86		BDL	11.4	BDL	0.61	2.21
2011 (I)	Fe†		65.80	13821	349	1710	1.48		55.8	1786	95.7	128	1.35
	Cu		BDL	43.3	3.17	4.45	1.17		BDL	28.8	3.54	4.56	1.07
	Zn	532	BDL	188	25.2	35.0	0.91	235	0.77	192	31.6	38.3	0.84
	Mn†		BDL	113	22.2	27.0	0.71		BDL	85.6	17.9	20.8	0.64
	Pb†		BDL	468	16.1	54.4	1.52		BDL	33.5	2.36	6.20	1.26
2011 (II)	Fe†		BDL	9022	71.9	374	2.24		BDL	26.3	10.2	9.82	0.57
	Cu†		BDL	60.9	8.41	10.0	0.84		BDL	17.1	5.56	5.55	0.65
	Zn†	880	BDL	252	14.2	23.7	1.26	293	BDL	27.5	5.14	5.87	0.90
	Mn†		BDL	259	8.89	22.4	1.52		BDL	22.7	BDL	2.66	1.49
	Pb†		BDL	70.0	BDL	1.86	3.47		BDL	3.51	BDL	0.08	5.05

† Significant difference between metal accumulation in the dermal tissue and the vascular bundle (Wilcoxon test, $p < 0.05$).

variance (c.v.) of Zn, Cu and Mn are all less than 1.3, much lower than that of Fe (1.30–2.24) and Pb (1.52–3.47). These results indicate that variations in Zn, Cu and Mn distributions in the dermal tissue are less than that of Fe and Pb (Table 1); they also suggest that the localization of these two groups of element may be controlled by different mechanisms.

In the vascular bundles, the accumulations of the metals are different from that in the dermal tissue. The average concentration of Zn is the highest, ranging from 5.87 ± 5.30 μg g^{-1} to 964 ± 666 μg g^{-1}, followed by Fe (9.82 ± 5.55 μg g^{-1} to 128 ± 172 μg g^{-1}), Mn (2.66 ± 3.95 μg g^{-1} to 50.8 ± 34.0 μg g^{-1}), Cu (4.56 ± 4.87 μg g^{-1} to 41.8 ± 15.6 μg g^{-1}) and Pb (0.08 ± 0.41 μg g^{-1} to 6.20 ± 7.82 μg g^{-1}) (Table 1). In particular, the concentrations of Fe and Pb in the vascular bundles are almost an order of magnitude lower than that in the dermal tissue, indicating that these two metals mainly accumulate in the dermal tissue of the root (Table 1, Fig. 1). As shown in Figs. 1(*e*)–1(*p*), bright rings of Mn, Cu and Zn are observed around the vascular bundles, where the Casparian strip is likely located. In a study by Lyubenova *et al.* (2012), the same bright ring structure was observed in the root sections of *T. latifolia* L. Therefore, the bright rings of Mn, Cu and Zn around the vascular bundles observed in this study likely suggest apoplastic transportation and accumulation of Mn, Cu and Zn around the Casparian strip. Synchrotron μXRF radiograph images (Fig. 3) show the heterogeneity of metal (Cu, Fe, Mn and Zn) distribution along a 1 cm-long root branch. Several 'hot spots' of metals are scattering across the branch. Therefore, heterogeneous distribution of metals could be observed not only across root sections but also along the axis of the root.

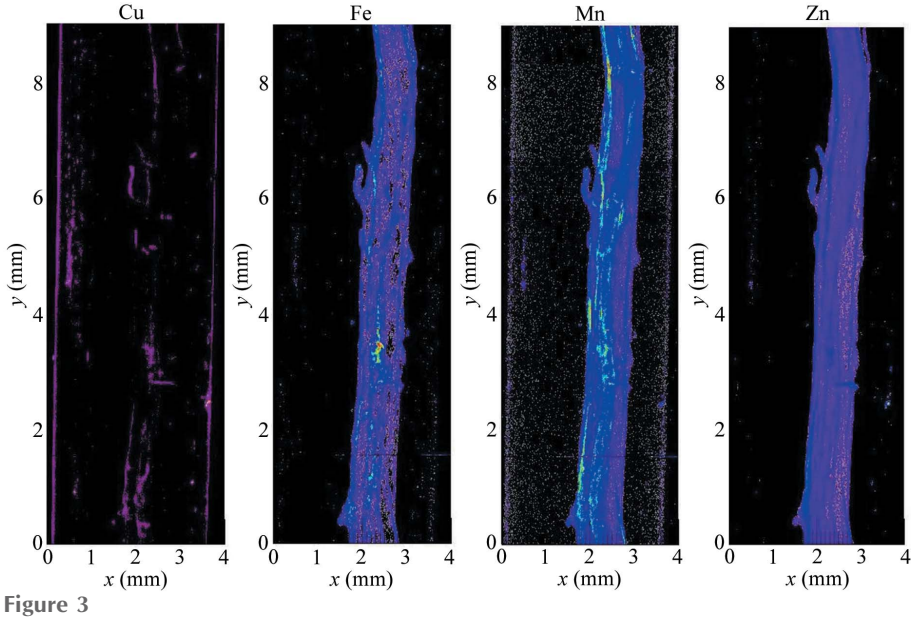

Figure 3
Spatial accumulation of Cu, Fe, Mn and Zn in the whole root collected in *T. latifolia* L. in 2010.

Table 2
Results of factor analysis based on localization of Cu, Fe, Mn, Pb and Zn in the dermal tissue and vascular bundle (rotated loading matrix, varimax rotation, gamma = 1.000).

Dermal tissues				Vascular bundles			
Parameter	Factor 1	Factor 2	Factor 3	Parameter	Factor 1	Factor 2	Factor 3
$\log_{10}$(Fe)	0.95	−0.07	0.13	$\log_{10}$(Zn)	0.92	−0.24	0.06
$\log_{10}$(Pb)	0.91	0.17	0.22	$\log_{10}$(Mn)	0.88	0.20	0.14
$\log_{10}$(Cu)	0.01	0.95	0.09	$\log_{10}$(Cu)	0.87	−0.22	−0.01
$\log_{10}$(Zn)	0.08	0.93	0.14	$\log_{10}$(Pb)	−0.12	0.97	0.15
$\log_{10}$(Mn)	0.25	0.18	0.95	$\log_{10}$(Fe)	0.09	0.14	0.99
% of total variance explained	35.7	36.4	20.0	% of total variance explained	47.9	21.9	20.3

3.3. Relationship between the localization of metals in dermal tissues and vascular bundles

Since the localization feature of metals is different between the dermal tissues and the vascular bundles (Fig. 1, Table 1), the mechanisms controlling the accumulation of metals in each tissue component should be examined. The association among Pb, Fe, Mn, Cu and Zn in their spatial distributions in both dermal tissues and vascular bundles were analyzed in order to investigate possible mechanisms governing the uptake and transportation of metals. As shown in Table 1, the coefficients of variance of metal concentrations in the tissues are greater than 0.5, suggesting a highly heterogeneous spatial accumulation of metals (Table 1). In order to reduce data skewness disturbing further statistical analysis, a logarithm ($\log_{10}$) transformation was applied to all of the data (McDonald, 2009). In addition, all four root samples were collected in the growing season and they shared the same mechanisms in the regulation of root metal accumulations (Tursun *et al.*, 2011). Therefore, the spatial distributions of Pb, Fe, Mn, Cu and Zn from all four samples were analyzed together. Factor analysis was performed to explore the internal relationships between the metal spatial accumulation in both dermal tissues and vascular bundles.

In the dermal tissue, three factors with eigenvalue greater than 0.5 are identified, which explain 92% of the total variance (Table 2). High loadings of Pb (0.95) and Fe (0.91) are observed in Factor 1 that explains 35.73% of the total variance, indicating close relationship between Pb and Fe in their spatial distribution in the root dermal tissues. Sequestration of Pb on wetland plant root surface with iron plaque has been observed in many studies (*e.g.* Liu *et al.*, 2007, 2011; Feng *et al.*, 2013). Therefore, Factor 1 represents the iron plaque in the dermal tissues. Factor 2, which has high loadings of Cu (0.95) and Zn (0.93), explains 36.42% of the total variance. This factor indicates a close association between the distribution of Zn and Cu in the dermal tissue, possibly because both elements are essential nutrients. Factor 3 accounts for 20.00% of the total variance with only one high loading element, Mn (0.95).

In the vascular bundles, three factors with eigenvalue greater than 0.5 are identified and explain 90.14% of the total variance (Table 2). Factor 1 explains 47.93% of the total variance. It has high loadings of Zn (0.92), Mn (0.87) and Cu (0.87), which are all essential nutrients for plant growth. The other two factors have high loading of only one specific metal in each factor. Factor 2 has high loading of Pb (0.97) and explains 21.89% of the total variance. Factor 3 has high loading of Fe (0.99) and explains 20.32% of the total variance (Table 2). The factor analysis suggested that the accumulations of metals in the dermal tissues and the vascular bundles were controlled by different mechanisms.

In order to investigate the differences in metal localization mechanisms between the dermal tissues and the vascular bundles, the associations between the spatial distribution of Cu, Mn, Pb, Fe and Zn in each type of tissue were further investigated. Simple linear regressions between the localization of metals in each specific type of root tissue were conducted to explore the association between metals.

4. Discussion

4.1. Effect of iron plaque on the spatial distributions of metals in dermal tissue

Because of the high affinity of metal cations to Fe hydroxide, iron plaque plays a role as either buffer or barrier of metals in the root uptake process. The role of iron plaque in the uptake of a metal can be judged based on the relationship between Fe and the metal in the iron plaque. If the correlation between Fe and the metal is strong in the iron plaque but weak in the regular dermal tissue, then iron plaque eliminates the uptake of this metal. If the correlation between Fe and the metal was weak in iron plaque but strong in regular dermal tissue, then iron plaque had no affinity to this metal. If the correlation between Fe and the metal was strong in both the iron plaque and the regular dermal tissue, it suggests that the iron plaque has strong affinity to the metal, but does not eliminate further transportation of the metal. In this case the iron plaque might be a buffer of the metal.

In this study a simple linear regression was applied to compare metal localization patterns (Cu, Mn, Pb and Zn) between iron plaque and regular dermal tissues (Fig. 4). According to Fig. 4, Pb has significant ($p < 0.05$) positive correlation with Fe in the iron plaque in all four root samples [Figs. 4(*a*)–4(*d*)] with $r^2 > 0.5$, suggesting a significant correlation between Fe and Pb in the iron plaque. However, the association between Fe and Pb in regular dermal tissues is rather weak (Fig. 4). As shown in Table 3, the concentration of Pb is rather low in the inner rim of the dermal tissue. In addition, extremely low accumulation of Pb is observed in the cortex tissues and the vascular bundles in this study (Table 1, Fig. 1), indicating that a very limited amount of Pb was transported to the rest of the plant tissues. Very likely, iron plaque acts as a barrier for the uptake of Pb in *T. latifolia* L.

Table 3
Accumulation (μg g^{-1}) of Fe in the iron plaque and regular dermal tissues from *T. latifolia* L. root sections collected in 2010 and 2011.

BDL = below detection limit.

	Iron plaque					Regular dermal tissues				
Sample	*n*	Min (μg g^{-1})	Max (μg g^{-1})	Median (μg g^{-1})	Mean ± SD (μg g^{-1})	*n*	Min (μg g^{-1})	Max (μg g^{-1})	Median (μg g^{-1})	Mean ± SD (μg g^{-1})
2010 (I)	404	187.00	33464	3720	4845 ± 4996	127	BDL	406	78.2	92.7 ± 73
2010 (II)	320	BDL	14667	810	1499 ± 2035	336	BDL	3765	158.0	261.0 ± 377
2011 (I)	250	439.00	13820	2517	3446 ± 2814	282	65.8	632	144.0	170 ± 87
2011 (II)	202	394.00	9021	856.0	1351 ± 1334	678	BDL	387.0	36.0	82.30 ± 95.6

Similar to Pb, the correlations between Fe and three essential elements (Mn, Zn and Cu) are significant ($p < 0.05$) in the iron plaque, indicating that iron plaque can co-precipitate these metals (Fig. 4). In the regular dermal tissues, however, the correlations of Mn, Zn and Cu with Fe are inconsistent. Both significant [Fig. 4(*e*), 4(*f*), 4(*h*)–4(*j*), 4(*l*), 4(*m*) and 4(*p*)] and insignificant [Figs. 4(*g*), 4(*k*), 4(*n*) and 4(*o*)] correlations are observed. The results suggest that Fe and the three other metals (Mn, Zn and Cu) may not share the same transport and accumulation mechanisms in the regular dermal tissues.

The effect of iron plaque on the localization of Cu, Mn and Zn in the root peripheral dermal tissue was further investigated by comparing the correlation among the three elements in the iron plaque and the regular dermal tissues (Fig. 5). Generally speaking, although the concentrations of

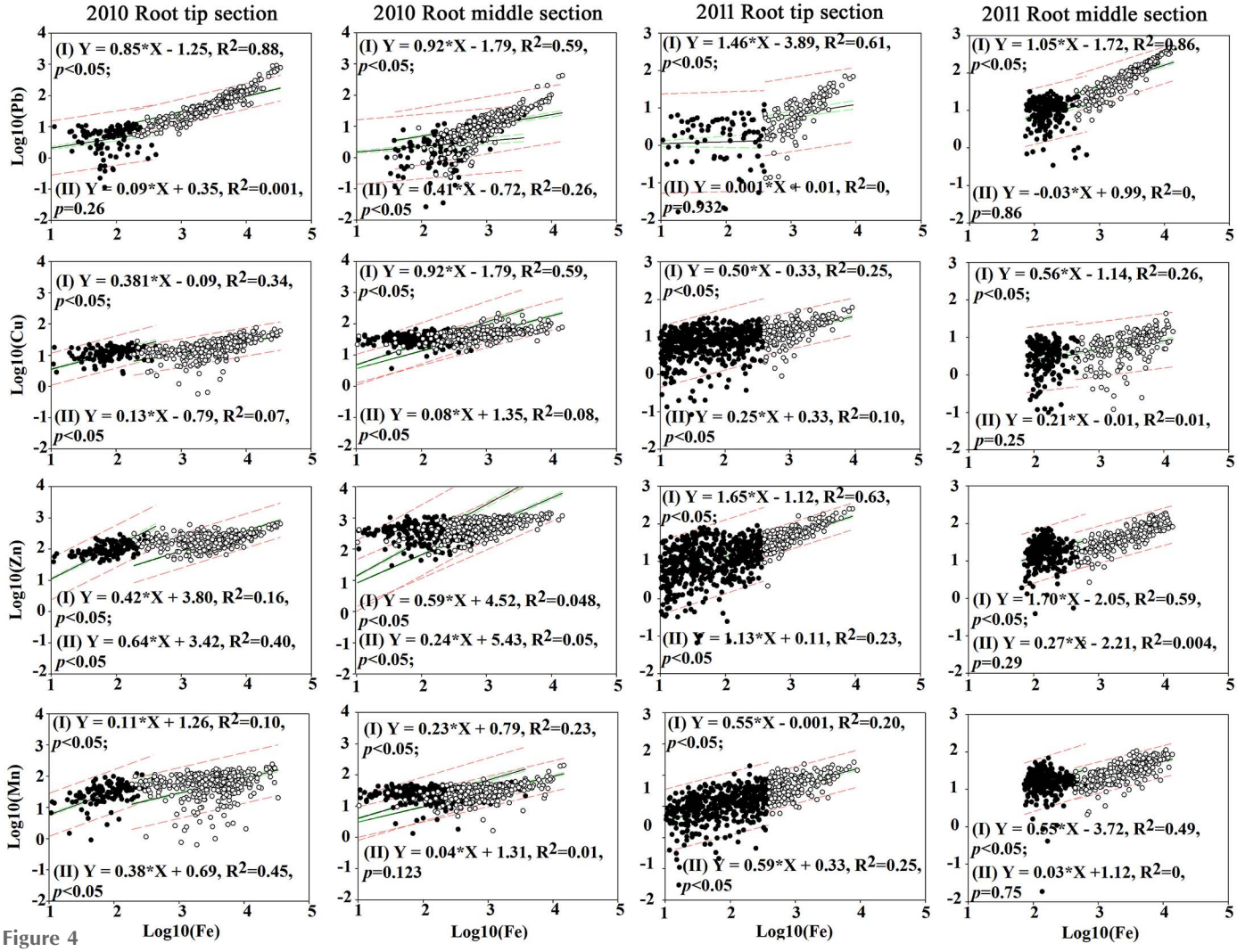

Figure 4
Linear regressions of Pb, Cu, Zn and Mn with Fe in the root tissue with iron plaque and the regular root dermal tissue. The *T. latifolia* L. samples were collected in 2010 and 2011, respectively. Regression line (I) is for the dermal root tissue with Fe plaque, and regression line (II) is for the regular root dermal tissue. Filled circles: regular root dermal tissue. Open circles: root dermal tissue with Fe plaque. Black lines: linear regression lines. Green dashed lines: 95% confidence level. Red dashed lines: 95% prediction band.

Mn, Zn and Cu are higher in the iron plaque, there is no obvious difference in the associations between the three elements in the iron plaque and the regular dermal tissues (Fig. 5). The association of metals with cell wall is determined by the concentration of metal cations in soil solution and the competition between metal cations (Schreiber & Franke, 2011). As shown in Fig. 5, the association between essential metals (Mn, Fe and Cu) is similar no matter whether it is in iron plaque or in the regular dermal tissues, suggesting that the accumulations of these metals is possibly controlled by the same mechanism. The only difference is that iron plaque adsorbs more Mn, Zn and Cu, causing high accumulation of these metals within the Fe plaque. These observations are consistent with previous studies conducted by St-Cyr & Campbell (1996) and Batty *et al.* (2000) who suggested that the adsorption and co-precipitation of Cu, Mn and Zn with iron plaque should not influence the further root uptake of these metals. Therefore, iron plaque possibly acts as a buffer for the accumulation of Mn, Zn and Cu in *T. latifolia* L.

4.2. Spatial distributions of metals in vascular bundles

Vascular bundles bridge the exchange of nutrients between roots and shoots and upload mineral nutrients from roots to shoots through xylem. In this study, high concentrations of Zn, Mn and Cu on the Casparian strip around the vascular bundles were observed (Fig. 1). Similar rings with high metal concentrations around the endodermis were also observed by Yamaguchi *et al.* (2011). They exposed *Solanum torvum* (Cd excluder) and *Sloanum melongena* (Cd accumulator) to a high concentration of Cd and found that the Cd concentration around the endodermis was higher in *Solanum torvum* than in *Sloanum melongena* (Yamaguchi *et al.*, 2011). Therefore, it is possible that the Casparian strip in the root may delay the transportation of Zn, Mn and Cu from apoplast to symplast.

In order to examine the similarity or difference in metal (Zn, Mn and Cu) accumulation mechanisms between the dermal tissues and the vascular bundles, the correlations between Zn and Mn, Zn and Cu, and Mn and Cu in both types of tissue were compared (Fig. 6). Significant ($p < 0.05$) positive correlations were observed between Mn and Zn, indicating the similar uptake and transport mechanisms between these two elements. In previous studies it was found that Zn and Mn could be taken up by *T. latifolia* L. from the rhizosphere soil more effectively than Cu (Sasmaz *et al.*, 2008; Klink *et al.*, 2012), and Mn and Zn usually shared the same transporters, such as ZIP and IRT1 in the root tissue (Hall & Williams, 2003).

The slopes of the regression lines for metal correlations show nearly no difference between the dermal tissues and the vascular bundles in most cases (Fig. 6). Different trends in the

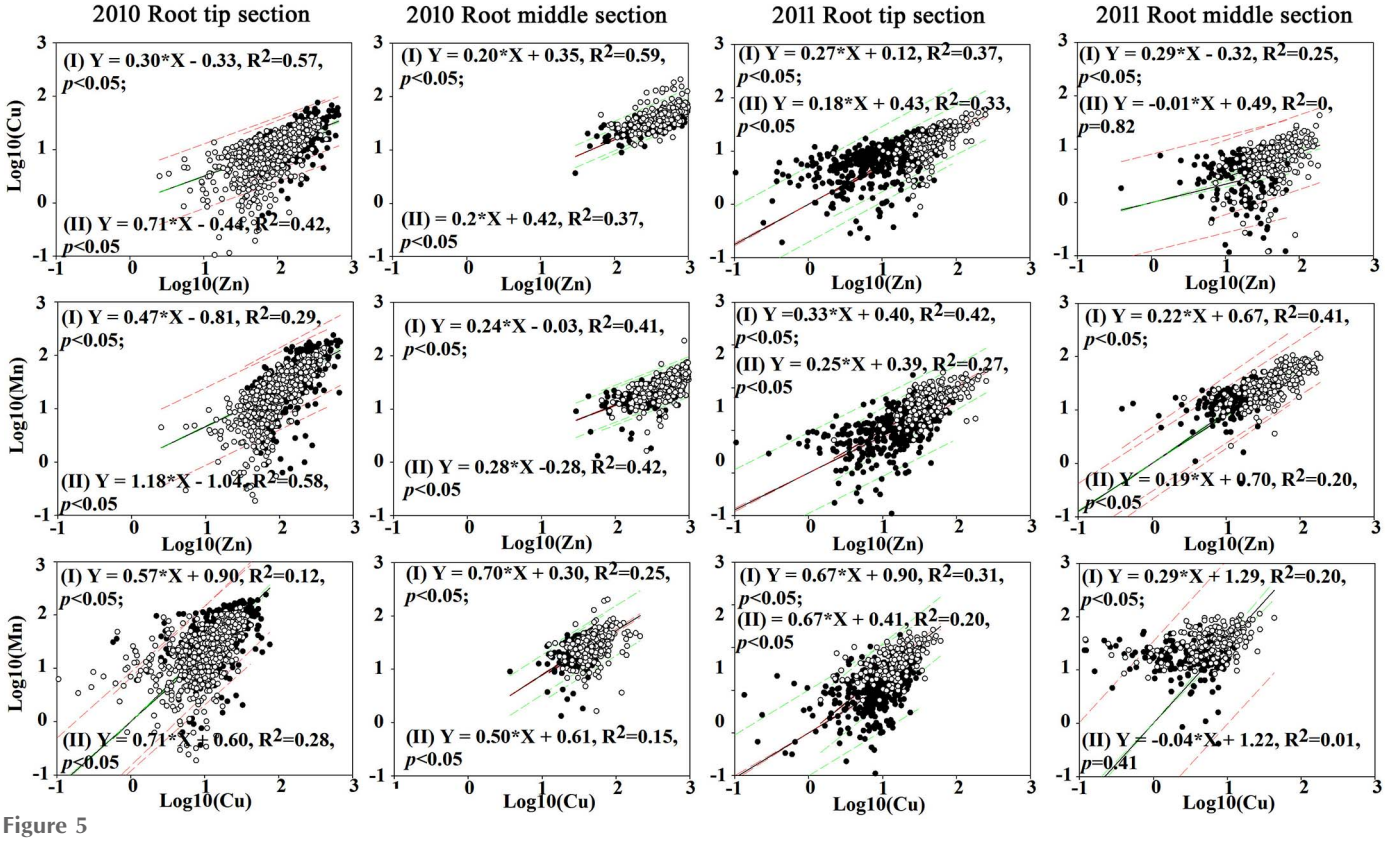

Figure 5
Linear regressions showing relationships between essential nutrients, *i.e.* Cu *versus* Zn, Mn *versus* Zn, and Mn *versus* Cu, in the dermal tissue with Fe plaque and the regular dermal tissue. The *T. latifolia* L. samples were collected in 2010 and 2011, respectively. Regression line (I) is for the dermal root tissue with Fe plaque, and regression line (II) is for the regular root dermal tissue. Filled circles: regular root dermal tissue. Open circles: root dermal tissue with Fe plaque. Black lines: linear regression lines. Green dashed lines: 95% confidence level. Red dashed lines: 95% prediction band.

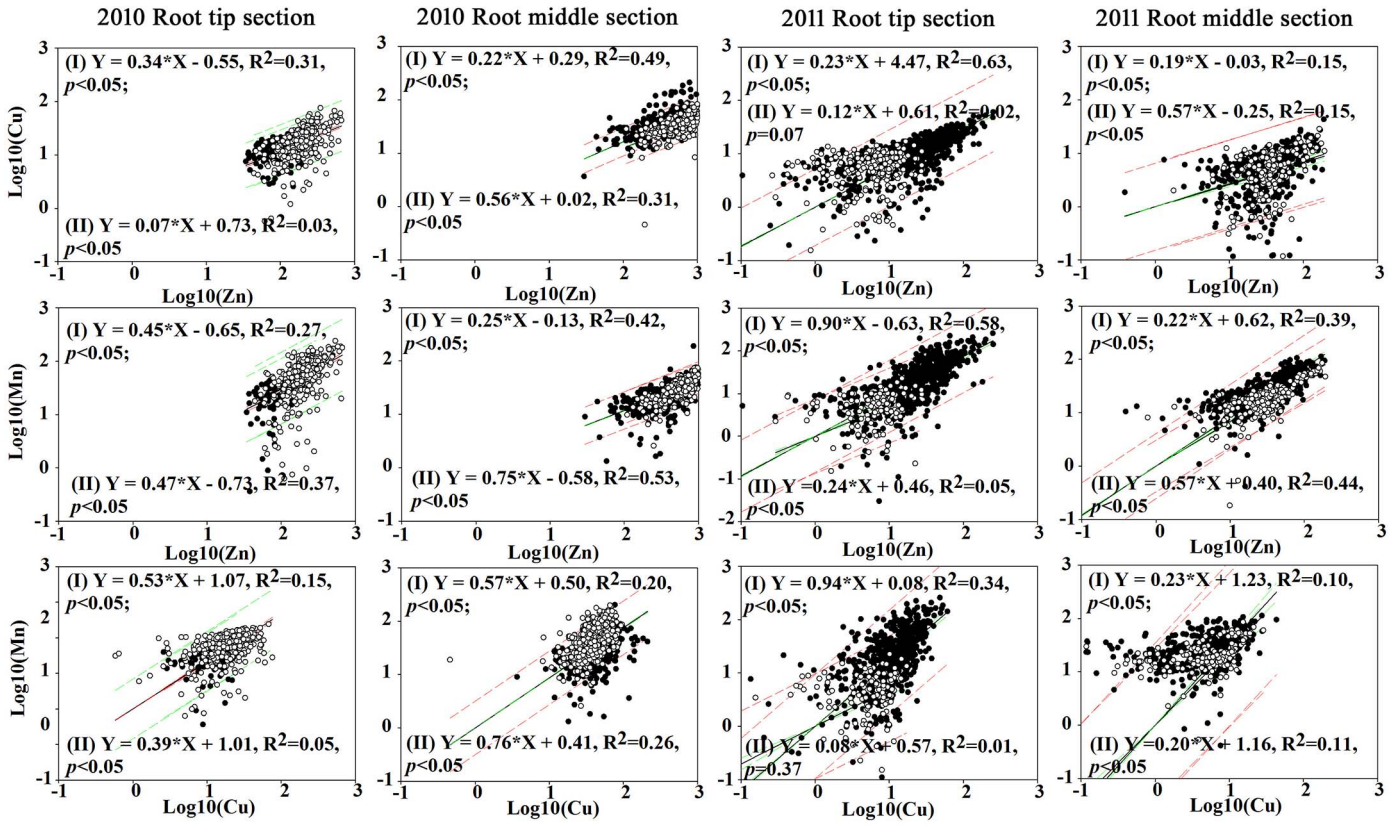

Figure 6
Linear regressions showing relationships between essential nutrients, *i.e.* Cu *versus* Zn, Mn *versus* Zn, and Mn *versus* Cu in the dermal tissue and the vascular bundle of *T. latifolia* L. The plant samples were collected in 2010 and 2011, respectively. Regression line (I) is for the root dermal tissue, and regression line (II) is for the root vascular bundle. Filled circles: root vascular bundle tissue. Open circles: root dermal tissue. Black lines: linear regression lines. Green dashed lines: 95% confidence level. Red dashed lines: 95% prediction band.

regression lines between the two types of tissues are only observed in a few cases [Fig. 6(*d*), 6(*h*) and 6(*l*)]. In addition, no distinct boundaries between the scatter plots from the two tissues are observed (Fig. 6). Therefore, the similar relationship of Zn, Cu and Mn between the dermal tissue and the vascular bundles indicate that these three elements accumulated in the two types of tissues possibly follow the same mechanism.

5. Conclusion

This study investigated the spatial distributions of Fe, Cu, Mn, Pb and Zn in *T. latifolia* L. roots during the growing season to explore possible mechanisms that govern metal localizations in root tissues. In the peripheral dermal tissues, the accumulations of metals in the roots were highly spatially heterogeneous and varied with the root tissue types and the metals themselves. There were significant correlations between the spatial distribution of Pb and Fe in the iron-plaque-enriched dermal tissues. At the same time, the correlations between Cu and Zn were significant in both iron-plaque-enriched dermal tissue and regular dermal tissues. Moreover, concentrations of Cu and Zn were higher in the iron-plaque-enriched dermal tissues, which suggests that iron plaque possibly acts as a barrier of Pb and a buffer of Zn and Cu in metal transport in dermal tissues. In the vascular bundles, significant correlations were observed between the spatial localization of Zn, Mn and Cu, especially between Mn and Zn, indicating the three metals may share similar localization mechanisms in the vascular bundles. Finally, the close association trends between the spatial distribution of Zn, Mn and Cu in the dermal tissues and the vascular bundles suggest that these two types of tissues may accumulate the three elements in a similar mechanism. This study demonstrates that the synchrotron XRF technique can provide an innovative approach to study metal assimilation in plants and explore the mechanism of plant metal uptake and transportation. The results can be used as a reference to advise biological modification of metal uptake and translocation rate of *T. latifolia* L. from a micro-scale perspective.

Acknowledgements

This work was supported in part by the China Scholarship Council (YQ) and the Margaret and Herman Sokol Foundation (HF). This project was also supported in part by the US Department of Energy, Office of Science, Office of Workforce Development for Teachers and Scientists (WDTS) under the Visiting Faculty Program (VFP) (HF). Use of the NSLS was supported by the US Department of Energy, Office of Science, Office of Basic Energy Sciences, under Contract No. DE-

AC02-98CH10886. NSLS X27A was supported in part by the US Department of Energy – Geosciences (DE-FG02-92ER14244 to The University of Chicago – CARS). We are also grateful to Dr Steve Heald, Co-editor of *Journal of Synchrotron Radiation*, and two anonymous reviewers who offered constructive comments and suggestions on an earlier draft of this paper.

References

Batty, L. C., Baker, A. J. M., Wheeler, B. D. & Curtis, C. D. (2000). *Ann. Bot.* **86**, 647–653.
Brennan, M. A. & Shelley, M. L. (1999). *Ecol. Eng.* **12**, 271–297.
Brunham, W. & Bendell, L. I. (2011). *Water Air Soil Pollut.* **219**, 417–428.
Burns, R. & Burns, R. (2008). *Business Research Methods and Statistics Using SPSS*. London: SAGE Publications.
Calheiros, C. S., Rangel, A. O. & Castro, P. M. (2009). *Bioresour. Technol.* **100**, 3205–3213.
Clemens, S., Palmgren, M. G. & Krämer, U. (2002). *Trends Plant Sci.* **7**, 309–315.
Desouki, S. H. & Feng, H. (2012). *Metal Contamination Sources, Detection and Environmental Impact*, edited by H. Shao, pp. 81–94. New York: NOVA Science Publishers.
Dickinson, N. M., Baker, A. J. M., Doronila, A., Laidlaw, S. & Reeves, R. D. (2009). *Int. J. Phytoremediat.* **11**, 97–114.
EPA (2005). *Guidance for Developing Ecological Soil Screening Levels*. US Environmental Protection Agency Office of Solid Waste and Emergency Response, Washington, DC 20460, USA.
Feng, H., Qian, Y., Gallagher, F. J., Wu, M., Zhang, W., Yu, L., Zhu, Q., Zhang, K., Liu, C. J. & Tappero, R. (2013). *Environ. Sci. Pollut. Res. Int.* **20**, 3743–3750.
Feng, H., Qian, Y., Gallagher, F., Zhang, W., Yu, L., Liu, C.-J., Jones, K. W. & Tappero, R. (2015). *J. Environ. Sci.* In the press.
French, C. J., Dickinson, N. M. & Putwain, P. D. (2006). *Environ. Pollut.* **141**, 387–395.
Gallagher, F. J., Pechmann, I., Bogden, J. D., Grabosky, J. & Weis, P. (2008). *Environ. Pollut.* **153**, 351–361.
Greipsson, S. & Crowder, A. (1992). *Can. J. Bot.* **70**, 824–830.
Grisey, E., Laffray, X., Contoz, O., Cavalli, E., Mudry, J. & Aleya, L. (2012). *Water Air Soil Pollut.* **223**, 1723–1741.
Hall, J. L. & Williams, L. E. (2003). *J. Exp. Bot.* **54**, 2601–2613.
Klink, A., Macioł, A., Wisłocka, M. & Krawczyk, J. (2012). *Limnologica*, **43**, 164–168.
Liu, J., Leng, X., Wang, M., Zhu, Z. & Dai, Q. (2011). *Ecotoxicol. Environ. Saf.* **74**, 1304–1309.
Liu, H. J., Zhang, J. L. & Zhang, F. S. (2007). *Environ. Exp. Bot.* **59**, 314–320.
Luo, X. S., Yu, S., Zhu, Y. G. & Li, X. D. (2012). *Sci. Total Environ.* **421–422**, 17–30.
Lyubenova, L., Pongrac, P., Vogel-Mikuš, K., Mezek, G. K., Vavpetič, P., Grlj, N., Kump, P., Nečemer, M., Regvar, M., Pelicon, P. & Schröder, P. (2012). *Metallomics*, **4**, 333–341.
Lyubenova, L., Pongrac, P., Vogel-Mikuš, K., Mezek, G. K., Vavpetič, P., Grlj, N., Regvar, M., Pelicon, P. & Schröder, P. (2013). *J. Hazard. Mater.* **248–249**, 371–378.
McDonald, J. H. (2009). *Handbook of Biological Statistics*. Baltimore: Sparky House Publishing.
McKenna, G. F. (1998). *Risk-Based Corrective Action and Brownfields Restorations*, edited by C. H. Benson, J. N. Meegoda, R. B. Gilbert and S. P. Clemence, pp. 16–29. Geotechnical Special Publication.
McNaughton, S. J., Folsom, T. C., Lee, T., Park, F., Price, C., Roeder, D., Schmitz, J. & Stockwell, C. (1974). *Ecology*, **55**, 1163–1165.
Marschner, P. (2012). *Marschner's Mineral Nutrition of Higher Plants*, 3rd ed. New York: Academic Press.
Qian, Y., Feng, H., Zhang, W., Yu, L., Zhu, Q., Zhang, L. & Wang, X. (2011). *Heavy Metal Sediments*, edited by L. H. Sanz, pp. 59–85. New York: NOVA Publishers.
Qian, Y., Gallagher, F. J., Feng, H. & Wu, M. (2012). *Environ. Pollut.* **166**, 23–30.
Rascio, N. & Navari-Izzo, F. (2011). *Plant Sci.* **180**, 169–181.
Sasmaz, A., Obek, E. & Hasar, H. (2008). *Ecol. Eng.* **33**, 278–284.
Schreiber, L. & Franke, R. B. (2011). *eLS*, doi: 10.1002/9780470015902.a0002086.pub2.
St-Cyr, L. & Campbell, P. G. (1996). *Biogeochemistry*, **33**, 45–76.
Taiz, L. & Zeiger, E. (2010). *Plant Physiology*. Sunderland, MA: Sinauer Associates.
Tripathi, R. D., Tripathi, P., Dwivedi, S., Kumar, A., Mishra, A., Chauhan, P. S., Norton, G. J. & Nautiyal, C. S. (2014). *Metallomics*, **6**, 1789–1800.
Tursun, N., Seyithanoglu, M., Uygur, F. N., Elibuyuk, I. O. & Elibuyuk, E. A. (2011). *Flora*, **206**, 731–735.
Wuana, R. A. & Okieimen, F. E. (2011). *ISRN Ecol.* **2011**, 1–20.
Yamaguchi, N., Mori, S., Baba, K., Kaburagi-Yada, S., Arao, T., Kitajima, N., Hokura, A. & Terada, Y. (2011). *Environ. Exp. Bot.* **71**, 198–206.
Ye, Z. H., Baker, A. J. M., Wong, M. H. & Willis, A. J. (1997). *New Phytol.* **136**, 469–480.
Ye, Z. H., Baker, A. J. M., Wong, M. H. & Willis, A. J. (1998). *Aquat. Bot.* **61**, 55–67.
Ye, Z. H., Cheung, K. C. & Wong, M. H. (2001). *Can. J. Bot.* **79**, 314–320.
Zhang, J., Tian, S., Lu, L., Shohag, M. J., Liao, H. & Yang, X. (2011). *J. Hazard. Mater.* **197**, 264–271.
Zhong, S., Shi, J. & Xu, J. (2010). *J. Soils Sediments*, **10**, 964–970.